Supplementary Information for

In-situ polymerized zwitterionic elastomers for efficient and stable perovskite solar cells

Wanli Li[a, b †], Yuheng Li[b, c†], Arnauld Robert Tapa[d], Minqiang Liu[e], Tie Liu[b], Haibing Xie[d], Yang Bai[e], Xiong Li[c], Zhongqin Xiao[f], Tao Yu[a, g], Zaiwei Wang[b, *] Chunxiong Bao[a, *] and Zhigang Zou[a, g]

[a] National Laboratory of Solid-State Microstructures, Collaborative Innovation Center of Advanced Microstructures, School of Physics, Nanjing University, Nanjing 210093, China

[b] Institute of Technology for Carbon Neutrality, Shenzhen Institute of Advanced Technology, Chinese Academy of Sciences, Shenzhen 518055, China.

[c] Michael Grätzel Center for Mesoscopic Solar Cells, Wuhan National Laboratory for Optoelectronics, Huazhong University of Science and Technology (HUST), Wuhan 430074, China.

[d] Institute for Advanced Study, Shenzhen University, Shenzhen 518060, China.

[e] Faculty of Materials Science and Energy Engineering, Shenzhen University of Advanced Technology, Shenzhen 518107, China.

[f] Bilight Intelligent manufacturing technology Co., Ltd. Dongguan 523000 China.

[g] Ecomaterials and Renewable Energy Research Center (ERERC), Jiangsu Provincial Key Laboratory for Nanotechnology, Nanjing University, Nanjing 210093, China

† These authors contributed equally: Wanli Li, Yuheng Li.

*Corresponding author E-mail:

cxbao@nju.edu.cn (C.B.)

zw.wang3@siat.ac.cn (Z.W.)

Table of contents

Experimental Section

Materials

Formamidinium iodide (FAI) was brought from Greatcell Solar Materials Pty LTD. Cesium iodide (CsI) and lead iodide (PbI_2) were purchased from Tokyo Chemical Industry (TCI). [6,6]-phenyl-C61-butyric acid methyl ester ($PC_{61}BM$) was purchased from Liaoning Youxuan New Energy Technology Co., LTD. Phenethylammonium iodide (PEAI), bathocuproine (BCP) and C_{60} were all purchased from Advanced Election Technology CO., LTD., China. (4-(7H-dibenzo[*c,g*]carbazol-7-yl)butyl)phosphonic acid (4PADCB) was purchased from Liwei New Material Technology Co., LTD. 2-methacryloyloxyethyl phosphorylcholine (MPC, 97%) and ammonium persulfate (APS) were purchased from Shanghai Aladdin Biochemical Technology Co., LTD. Al_2O_3 dispersions (30 nm 20 w.t.% in isopropanol), N,N-dimethylformamide (DMF), dimethyl sulfoxide (DMSO) and isopropanol (IPA), Chlorobenzene (CB) were purchased from Sigma Aldrich. All the chemicals were purchased from commercial vendors without further purification.

Preparation of zwitterionic elastomer

First, 295 mg MPC was dissolved in 300 μL deionized water and completely dissolved by ultrasound at room temperature for 10 min. Then 3 mg APS as initiator was added and completely dissolved by ultrasound at room temperature for 10 min. Finally, the elastomer, as shown in Supplementary Fig. 2, can be obtained by heating the mixed solution water bath for 1 h.

Perovskite precursor solutions

1.53 eV bandgap perovskites. For the composition $FA_{0.95}Cs_{0.05}PbI_3$, 1.5 M perovskite precursor solution was prepared by mixing CsI, FAI and PbI_2 in DMF: DMSO = 4:1 (vol/vol) mixed solvent subject to the stochiometric ratio. Additional 3 mol% PbI_2 and

10 mol% MACl were added to the precursor for better crystallization and perovskite phase transformation. The precursor solutions were stirred at room temperature for 2 h and then filtered using a 0.22 polytetrafluoroethylene membrane before use. For $FA_{0.95}Cs_{0.05}PbI_3$/MPC precursor solution, 10 mg of MPC was first dissolved in 1 ml DMSO solution, then 0.5 mg of APS was added as initiator. Then 25 μL of the above mixed solution was added in 500 μL pristine $FA_{0.95}Cs_{0.05}PbI_3$ precursor solution. In studies comparing different concentration additive, we optimized the concentration of MPC, testing 0.25, 0.5, 0.75, and 1 mg ml^{-1}, finding that 0.5 mg ml^{-1} is the best concentration for MPC.

1.85eV bandgap perovskites. For the composition $Cs_{0.06}FA_{0.66}MA_{0.28}Pb(I_{0.5}Br_{0.5})_3$, 1.0M perovskite precursor solution was prepared by mixing CsI, MABr, FAI, PbBr and PbI_2 in DMF: DMSO = 4:1 (vol/vol) mixed solvent subject to the stochiometric ratio. The precursor solutions were stirred at room temperature for 2 h and then filtered using a 0.22 polytetrafluoroethylene membrane before use. For $Cs_{0.06}FA_{0.66}MA_{0.28}Pb(I_{0.5}Br_{0.5})_3$ /MPC precursor solution, MPC solution containing APS at a concentration of 0.5 mg/mL was added to the perovskite precursor.

1.25eV bandgap mixed tin–lead perovskites. The $Cs_{0.1}FA_{0.6}MA_{0.3}Pb_{0.5}Sn_{0.5}I_3$ perovskite precursor solution was prepared by mixing CsI (0.18 mmol), FAI (1.08 mmol), MAI (0.54 mmol), SnI_2(0.9 mmol), PbI_2 (0.9 mmol), SnF_2 (0.09 mmol) and NH_4SCN (1.5 mg) in a solvent mixture of 0.25 ml DMSO and 0.75 ml DMF to reach a concentration of 1.8 M for the control samples. The precursor solutions were stirred at room temperature for 2 h and then filtered using a 0.22 polytetrafluoroethylene membrane before use. For the MPC samples, MPC solution containing APS at a concentration of 0.5 mg/mL was added to the control materials.

Device fabrication

1.53 eV bandgap perovskite solar cells. Prepatterned ITO glasses were cleaned sequentially with detergent, deionized water, acetone, and ethanol under sonication for 30 min, respectively. Then they were blown dry with nitrogen and treated with ultraviolet ozone treatment for 30 min before using. The hole transport layer (HTL) was fabricated by using SAM solution of 4PADCB. The 4PADCB concentration is 0.5 mg ml^{-1} in ethanol solution and spin-coated on ITO at 3000 rpm. for 30 s, followed by annealing at 100 °C for 10 min. The isopropanol solution of Al_2O_3 was diluted 1:50 with isopropanol, shaken at room temperature for 30 min, and then spin-coated directly on top of the SAM surface at 5000 rpm for 30 s and subsequently annealed at 100 °C

for 5 min. The perovskite precursor (50 µL) was spin-coated at 2000 rpm for 10s and 4000 rpm for 40s. At 10 s before the end of the spinning, 150 µL CB was dropped as antisolvent. The film was immediately annealed at 100 °C for 30 min. Then for the passivation treatment, 1.5 mg PEAI and 0.5 mg $EDAI_2$ was dissolved in 1 mL isopropanol solvent, shocked overnight and filtered before use, 50 µL mixed solution was dynamic spin-coated on the perovskite films at 3000 rpm for 30 s, followed by annealing at 100 °C for 5 min. After cooling down to room temperature, the substrates were transferred to the evaporation system and a 20 nm C_{60} film was subsequently deposited on top by thermal evaporation at a rate of 0.2 A s^{-1}, after finishing the C_{60} deposition, the substrates were then transferred to the atomic layer deposition (ALD) system to deposit 20 nm SnO_2 at 100 °C. Finally, 100 nm Ag electrode was evaporated by thermal evaporation.

1.85 eV bandgap perovskite solar cells. The steps prior to the deposition of the perovskite layer were identical to those used for the fabrication of the 1.53 eV perovskite solar cell. Next, the perovskite precursor (50 µl) was spin-coated at 1,000 rpm for 10 s (2 s acceleration to 1,000 rpm) and 4000 rpm for 30 s (2 s acceleration to 4000 rpm). 150 µl anisole was dropped on the film 5 s before the end of the spinning programme. The film was immediately annealed at 100 °C for 10 min. For the interfacial passivation layer, a solution, with 0.5 mg $EDAI_2$ and 1 mg PEAI added to 1 ml IPA, was spin-coated onto the as-prepared perovskite films and followed up with 5 min thermal annealing under 100 °C. The as-prepared perovskite films were transferred into an evaporation chamber. Subsequently, 20 nm of C_{60} and 7 nm of BCP were thermally evaporated onto them. Finally, a 100 nm thick Ag layer was evaporated as the back electrode.

1.25 eV bandgap perovskite solar cells. The steps prior to the deposition of the HTL were identical to those used for the fabrication of the 1.53 eV perovskite solar cell. Next, PEDOT: PSS diluted with IPA (1:2, v/v) was spin-coated onto the ITO substrates at 4000 rpm for 30 s and annealed at 100°C for 10 min. 50 µL of $Cs_{0.1}FA_{0.6}MA_{0.3}Pb_{0.5}Sn_{0.5}I_3$ precursor solutions were spin-coated on each substrate at 1000 rpm for 10 s and then at 4000 rpm for 30 s. 150 µl anisole was dropped on the film 15 s before the end of the spinning programme. The obtained perovskite films were then annealed on a hot plate at 100 °C for 10 minutes. Followingly, 60 µL of $EDAI_2$ solutions (dissolved in IPA at a concentration of 0.5 mg mL-1) were dropped onto the perovskite films and spin-coated at 5000 rpm for 30 s and annealed on a hot plate at

100 °C for 5 minutes. The as-prepared perovskite films were transferred into an evaporation chamber. Subsequently, 20nm of C_{60} and 7 nm of BCP were thermally evaporated onto them. Finally, a 100 nm thick Ag layer was evaporated as the back electrode.

Perovskite solar mini-module fabrication

The perovskite solar modules （PSMs） consisting of 7 sub-cells connected in series were fabricated on ITO glass substrates with dimensions of 5.0 cm × 5.0 cm. The series interconnection of the mini-module was accomplished by means of P1, P2, and P3 lines, which were scribed with the Maike Xianna/PLSS10 green picosecond laser scribing system. P1 lines (a width of 20 μm) were pre-patterned on the ITO glass substrates by utilizing 28% of a laser power under a speed of 50 mm/s with a frequency of 500 kHz and a pulse duration of 120 ns. The ITO substrate was cleaned with organic solvent and treated with UVO for 30 min. Compared to the fabrication of hole transport layer (HTL), perovskite and surface passivation layers for small area solar cells, except for a corresponding increase in the amount of solution, other parameters remain unchanged. Subsequently, 20 nm C_{60} and 20 nm SnO_2 were sequentially thermal evaporated and atomic layer deposition onto these perovskite films. Before the Ag electrode deposition process step, the P2 lines （a width of 100 μm） were patterned. This was accomplished at an average laser power of 24% under a speed of 100 mm/s with a frequency of 500 kHz and a pulse duration of 120 ns. When the 100 nm thick Ag electrode was deposited, the P3 lines (a width of 80 μm) were patterned by utilizing 25.5% of a laser power under a speed of 200 mm/s with a frequency of 500 kHz and a pulse duration of 120 ns.

Sample characterization

The dynamic light scattering (DLS) was used to calculate the colloid size distribution in perovskite precursor solutions by Malvern Nano ZS90. Proton Nuclear Magnetic Resonance (1H-NMR) spectra were measured using a Bruker AVANCE NEO-400 NMR spectrometer. Fourier-transform infrared (FTIR) spectra were measured with a Shimadzu IR Affinity-1 spectrometer. X-ray photoelectron spectroscopy (XPS) was carried out by Thermo K-Alpha+. The UV-vis absorption spectra were measured by Shimadzu UV2600i spectrophotometer. The photoluminescence (PL) and time-resolved photoluminescence (TRPL) spectra were measured with 400 nm pump pulse by an Edinburgh FS5 spectrofluorometer. The surface roughness and potential were

tested using a Jupiter XR Atomic Force Microscope (AFM, Oxford Instruments) with a tapping amplitude modulation mode. The scanning electronic microscope (SEM) images were obtained from Zeiss GeminiSEM 500 ultra-high-resolution FE-SEM system. High resolution transmission electron microscope (HRTEM) images were obtained using a JEOL JEM-F200 field-emission gun microscope with a 0.10-nm point to-point resolution at 200.0 kV. The diffraction patterns of perovskite films were implemented by X-ray diffraction (XRD, MiniFlex600, Rigaku). The grazing incidence X-ray diffraction (GIXRD, Rigaku SmartLab) was utilized to characterize the residual tensile thermal stress of perovskite films. Grazing incidence wide angle X-ray scattering (GIWAX) spectra were obtained by BL14B1 beamline of the Shanghai Synchrotron Radiation Facility (SSRF). Contact angle tests were measured by Krüss DSA30 optical contact angle meter. ToF- SIMS measurements were performed on a TOF-SIMS5-100. Cs^+ was used as a sputtering ion with 1 keV ion energy, 55 nA ion current, and 300 ×300 μm^2 raster size. While analysis was carried out using a pulsed primary ion beam of Bi^{3+} (30 keV). An area of 100 ×100 μm^2 was measured.

Device characterization

The photovoltaic performance of the device was measured under the simulated solar lamp (100 mW cm^{-2}, AM 1.5G) provided by Enli Tech 3A 450 W solar simulator. The J-V curves of PSCs were measured at room temperature. The light source parameters are 450 W xenon lamp (Enli Tech solar simulator). Light intensity was calibrated with a standard silicon cell (IVS-KA6000-2022, EnliTech). Size of the mask used during testing was 0.048 cm^2. The scanning parameters were forward scanning (1.2 to -0.1V, step 0.01V, delay time 100 ms) and reverse scanning (from -0.1 to 1.2 V, step 0.01 V, delay time 100 ms). The external quantum efficiency (EQE) was measured in ambient air using the solar-cell-spectra-response measurement system (QE-R, EnliTech). The transient photovoltage (TPV), transient photocurrent (TPC) curves and Mott-Schott were measured by a multifunctional optoelectronic test system (PIAOS, Swiss). The EQE of electroluminescence (EQE_{EL}) spectra of the PSCs were detected by ENLITECH REPS-VOC under dark conditions. For the temperature cycling tests, the encapsulated PSCs were placed in the high and low temperature alternating damp heat test chamber (THS-C100-II, Zhetu, China), with the temperature cycling between -40 ℃ to 85 ℃. The temperature change rate between the -40 ℃ and 85 ℃, the heating rate was set at 1 °C, the cooling rate at 0.7 °C, and a single test cycle lasted approximately 5 hours. The encapsulated devices were measured periodically in an

N2-filled glove box after the devices cooling down. Operational stability test: The operational stability of the unencapsulated devices is tested at the MPP tracking under simulated 1 sun illumination (LED solar simulator). There is an interval of 20 min for data collection. During the MPP tracking, the device is performed in ambient conditions. Thermal-humidity test: The devices were placed in ambient under dark with 85 °C.

Theory Calculation

We first optimized the structure of MPC monomer (i.e., the minimal structural unit) using density functional theory's B3LYP-GD3BJ/6-31G(d) under Gauss View 5.0 and Gaussian 09W software[1]. The vibrational frequencies of the optimized structures were carried out at the same level. The structures were characterized as a local energy minimum on the potential energy surface by verifying that all the vibrational frequencies were real. The Visual Molecular Dynamics (VMD) program was used to plot the color-filled iso-surface graphs to visualize the molecular electrostatic potential (ESP)[2]. The Vienna Ab Initio Package (VASP) was employed to perform all the density functional theory (DFT) calculations within the generalized gradient approximation (GGA) using the Perdew, Burke, and Enzerhof (PBE) formulation[3, 4]. To address van der Waals interactions between the adsorption atom and layers, we employed the DFT-D3 method[5], which effectively handles remote dispersion interactions. The interaction between electrons and ions was modeled using the projector augmented wave (PAW) method with plane waves up to a cutoff energy of 400 eV[6]. The electron self-consistency convergence criterion was set at 10^{-5} eV. Since we added an excess of PbI_2 combined with XRD results, the (100) surface of $FAPbI_3$ was chosen PbI2-terminated surfaces have been constructed. The slab models have a 5×2×2 periodicity, and a 30 Å vacuum region was added. To describe the thermodynamic stability of the defect, the defect formation energy (E_f) was defined as:

$$E_f = E_{defect} - E_{perfect} - \sum n_i \mu_i \quad (1)$$

where E_{defect} is the energy of the defective surface, $E_{perfect}$ is the total energy of the perfect surface, n_i represents an increase in the number of I atoms as a replacement or a decrease in the number of Pb atoms at (100) surface, and μ_i is the chemical potential corresponding to the I species.

We calculated the adsorption energies of the molecules on the surface with V_I

defect, V_{Pb} defect, The adsorption energy (E_{abs}) was defined as:

$$E_{abs} = E_{total} - E_{surf} - E_{A(g)} \quad (2)$$

where E_{abs}, E_{total}, and $E_{A(g)}$ are the energy of adsorbate A adsorbed on the surface, the energy of a clean surface with or without defect, and the energy of isolated A molecule in a cubic periodic box, respectively.

Supplementary Notes

Note S1 Residual Stress Analysis

The film stress can be calculated according to the Bragg's Law and generalized Hooke's Law, the 2θ-$sin^2\Psi$ can be given by:[7]

$$\sigma = -\frac{E}{2(1+\upsilon)}\frac{\pi}{180}cot\theta_0\frac{\partial(2\theta)}{\partial sin^2\Psi} \quad (3)$$

where E represents the perovskite modulus (10 GPa) and υ denotes Poisson's ratio of the perovskite (0.3), respectively. θ_0 indicates the diffraction peak for a strain-free perovskite crystal plane, while θ is the diffraction peak for the measured perovskite films. Ψ signifies the angle of the diffraction vector in relation to the normal direction of the sample.

Note S2 Williamson-Hall Analysis

We assessed the variation of micro-strains utilizing the Williamson-Hall equation:[8]

$$\beta \times cos\theta = \frac{K\lambda}{D} + 4\varepsilon \times sin\theta \quad (4)$$

where D, ε, θ, β, *K* and λ represent the crystallite size and lattice distortion of perovskite films, the FWHM of diffraction peaks, half of the scattering angle, the shape factor, and the wavelength of the incident X-rays (1.5406 Å), respectively.

Note S3 Exciton lifetime calculation

The exciton lifetime of the perovskite films can be derived from the femtosecond transient absorption spectroscopy (TAS) utilizing a bi-exponential fitting aapproach, as shown in the following equation:

$$y = y_0 + A_1 e^{\left(-\frac{t}{\tau_1}\right)} + A_2 e^{\left(-\frac{t}{\tau_2}\right)} \quad (5)$$

$$\tau_{avg} = \frac{A_1{\tau_1}^2 + A_2{\tau_2}^2}{A_1\tau_1 + A_2\tau_2} \quad (6)$$

where y_0 is constant, τ_1 and are the decay components of the trap-assisted and radiative recombination process respectively. τ_{avg} represents the average carrier recombination lifetime.

Note S4 Light intensity-dependent V_{OC} analysis

$$V_{OC} = \frac{nk_BT}{q}\ln(I) + B \quad (7)$$

where k_B, *T, q, I, B* represent Boltzmann constant, thermodynamic temperature, the electron charge, light intensity and constant, respectively. The smaller n is theoretically, the indirect defect recombination at the interface (SRH recombination, Shockley-Read-Hall recombination) is smaller.

Note S5 FF losses analysis

$$FF_{max} = \frac{v_{oc} - ln(v_{oc} + 0.72)}{v_{oc} + 1} \quad (8)$$

$$\text{with} \quad v_{oc} = \frac{qV_{oc}}{nk_BT} \quad (9)$$

where k_B, T, q, n represent Boltzmann's constant, Kelvin temperature, electron charge, and the ideality factor, respectively.

Note S6 Temperature dependent conductivity calculation

The activation energy (E_a) can be derived from the slope of the $\ln(\sigma T)^{-1}/k_BT$ relation extracted from the temperature-dependent ion conductivity by the Nernst–Einstein relation.

$$\sigma(T) = \sigma_0 T exp(-E_a/k_BT) \quad (10)$$

where k_B is the Boltzmann constant, σ_0 is a constant, and T is absolute temperature[9].

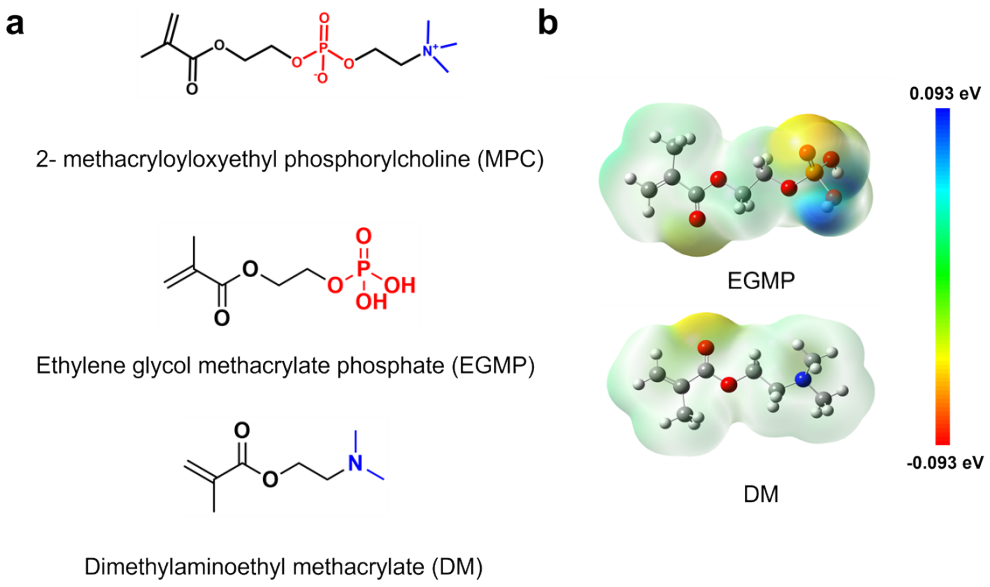

Fig. S1. (a) Schematic molecular structure of DM, EGMP and MPC. (b) ESP maps of DM, EGMP.

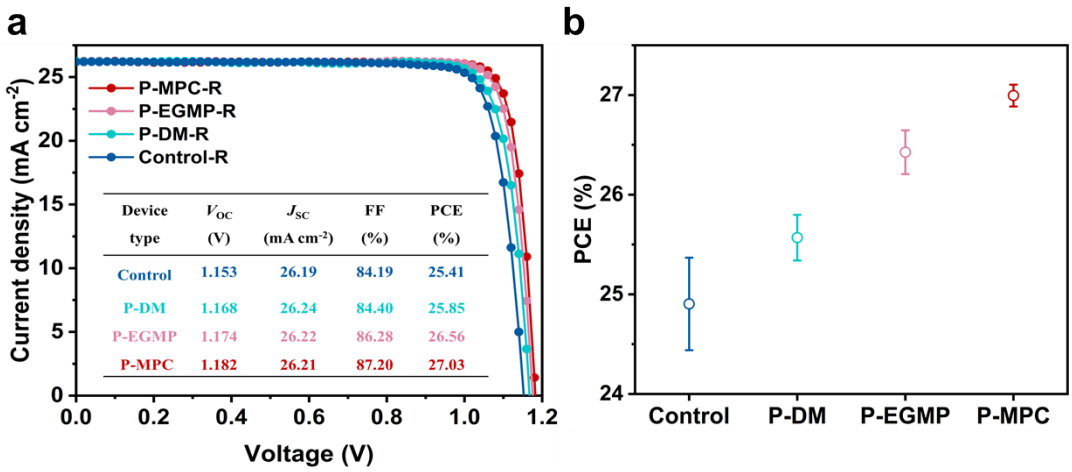

Device type	V_{OC} (V)	J_{SC} (mA cm^{-2})	FF (%)	PCE (%)
Control	1.153	26.19	84.19	25.41
P-DM	1.168	26.24	84.40	25.85
P-EGMP	1.174	26.22	86.28	26.56
P-MPC	1.182	26.21	87.20	27.03

Fig. S2. (a) J-V curves and photovoltaic parameters of control, P-DM, P-EGMP and P-MPC devices. (b) PCE of the control, P-DM, P-EGMP and P-MPC PSCs. The PCEs are presented as mean ± s.d. from 10 independent devices per condition.

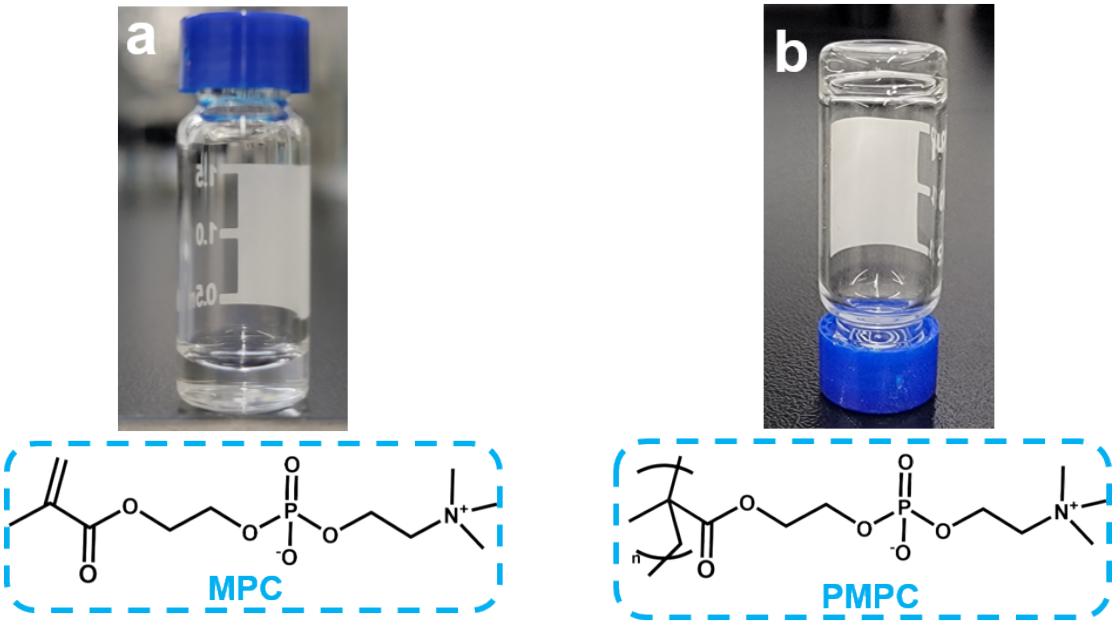

Fig. S3. The picture of MPC (including APS as the initiator) before (a) and after (b) heating at 100 ℃

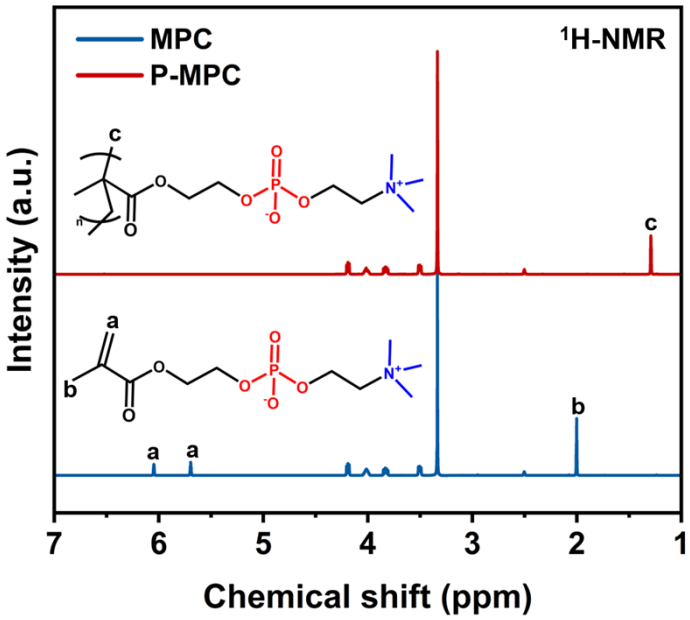

Fig. S4. ^{1}H NMR spectra of MPC and P-MPC

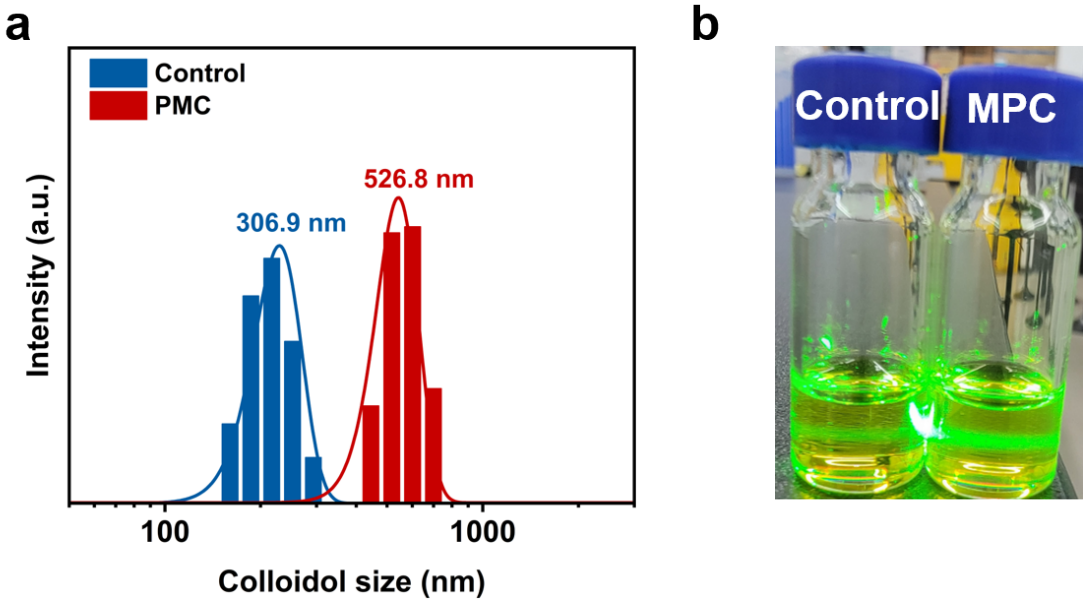

Fig. S5. Dynamic Light Scattering (DLS) spectra of the control and MPC-modified precursor

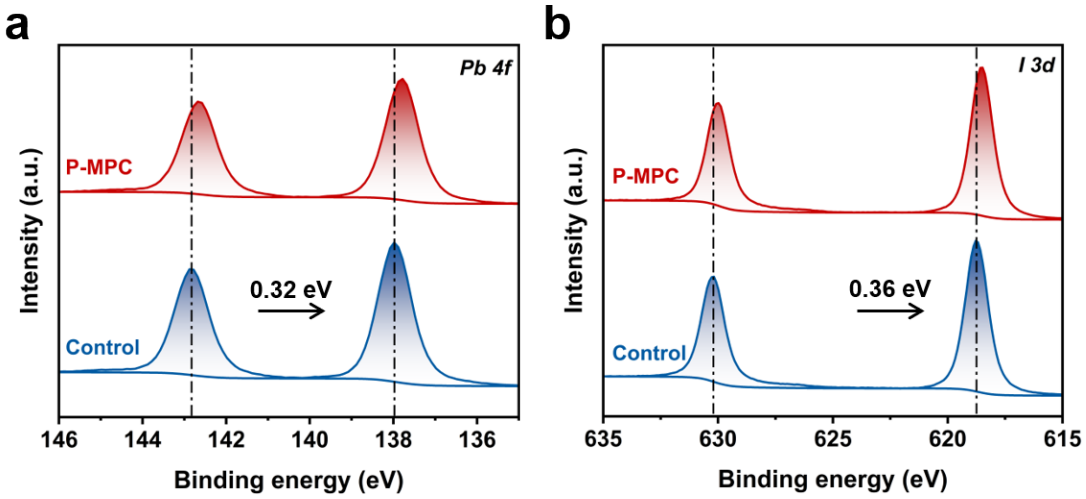

Fig. S6. XPS spectra of Pb 4f and I 3d of the control and P-MPC perovskite films, respectively.

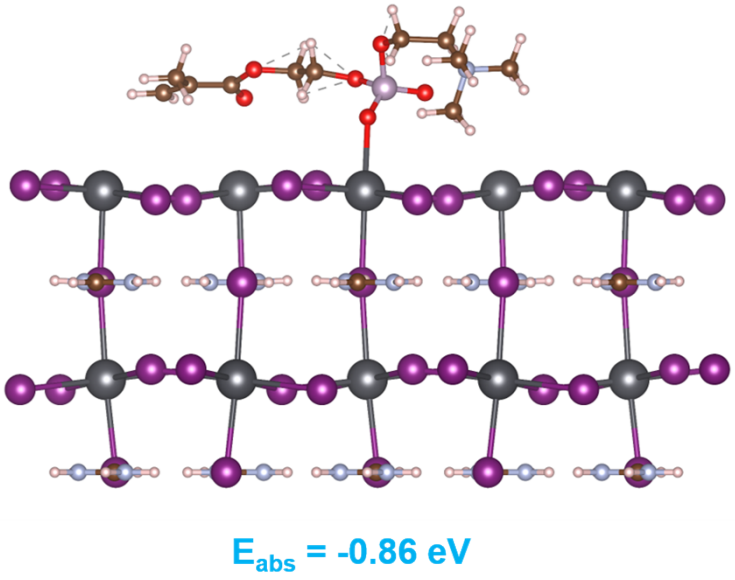

Fig. S7. The structure of MPC adsorbed on the surface of perovskite.

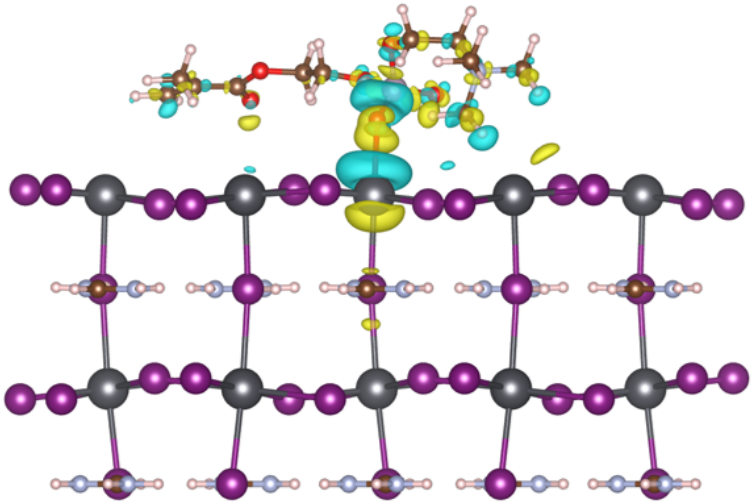

Fig. S8. Differential charge density of MPC adsorbed on the surface of perovskite.

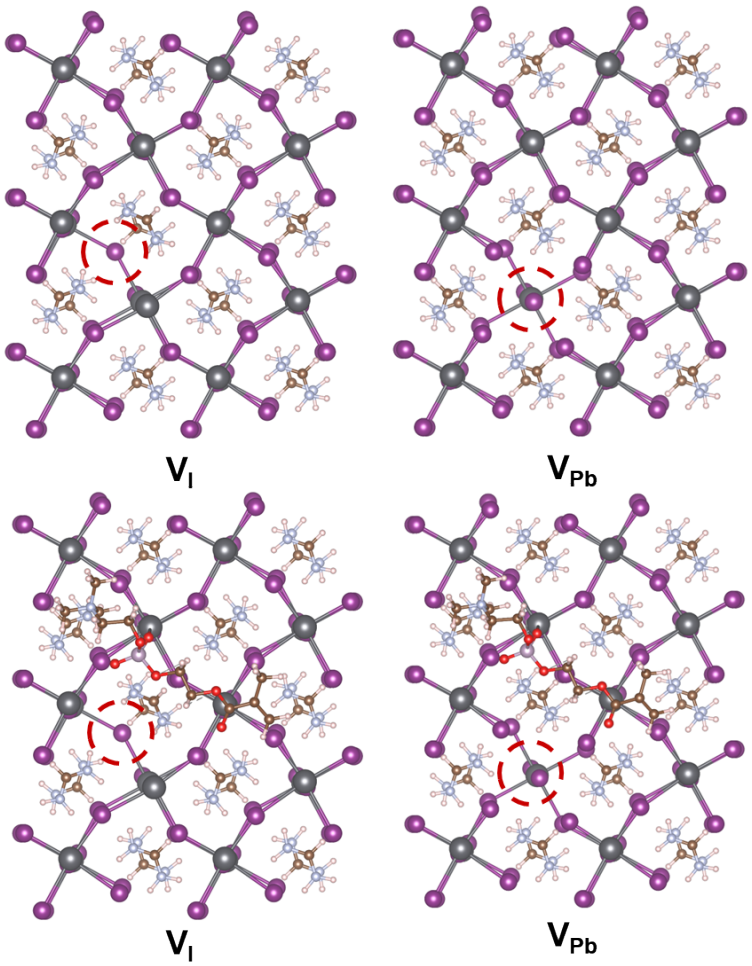

Fig. S9. Schematic diagrams of two crystal defects before and after perovskite-MPC composite.

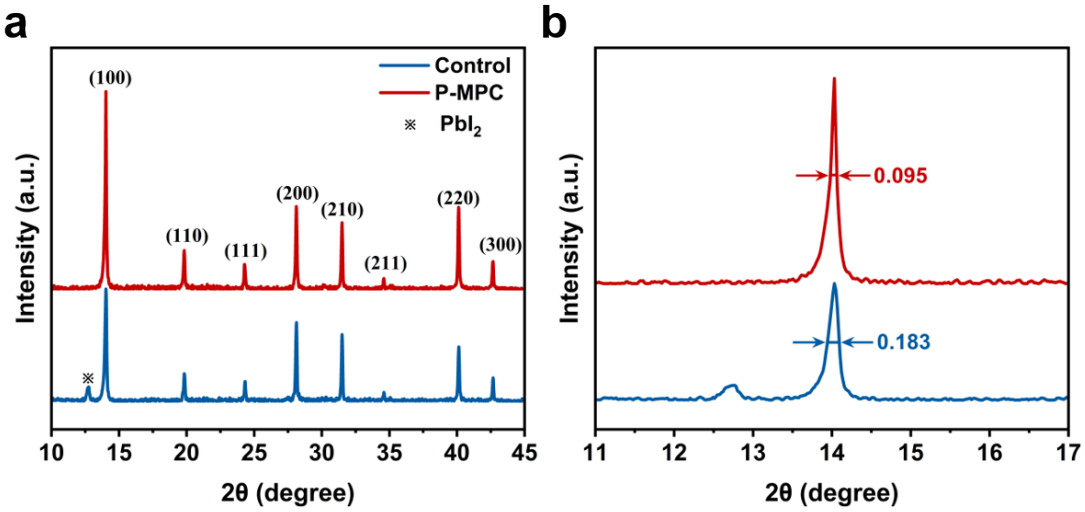

Fig. S10. X-ray diffraction patterns of control perovskite film and perovskite film with P-MPC.

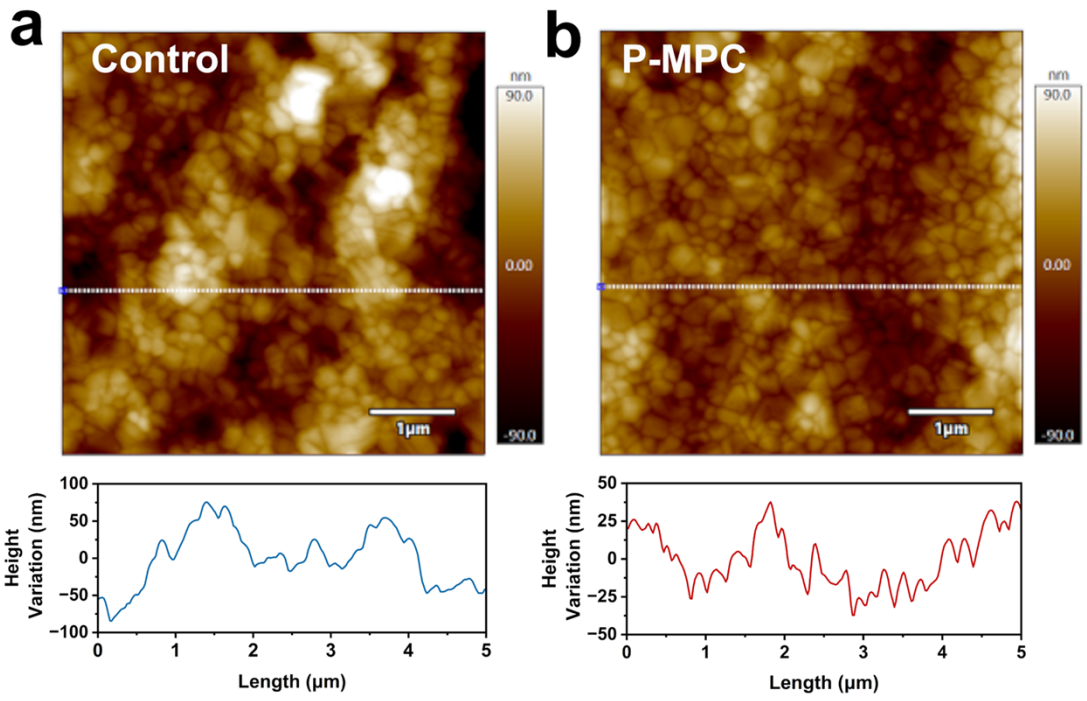

Fig. S11. (a) and (b) AFM images and the corresponding height along the line profiles of control and P-MPC perovskite films, respectively.

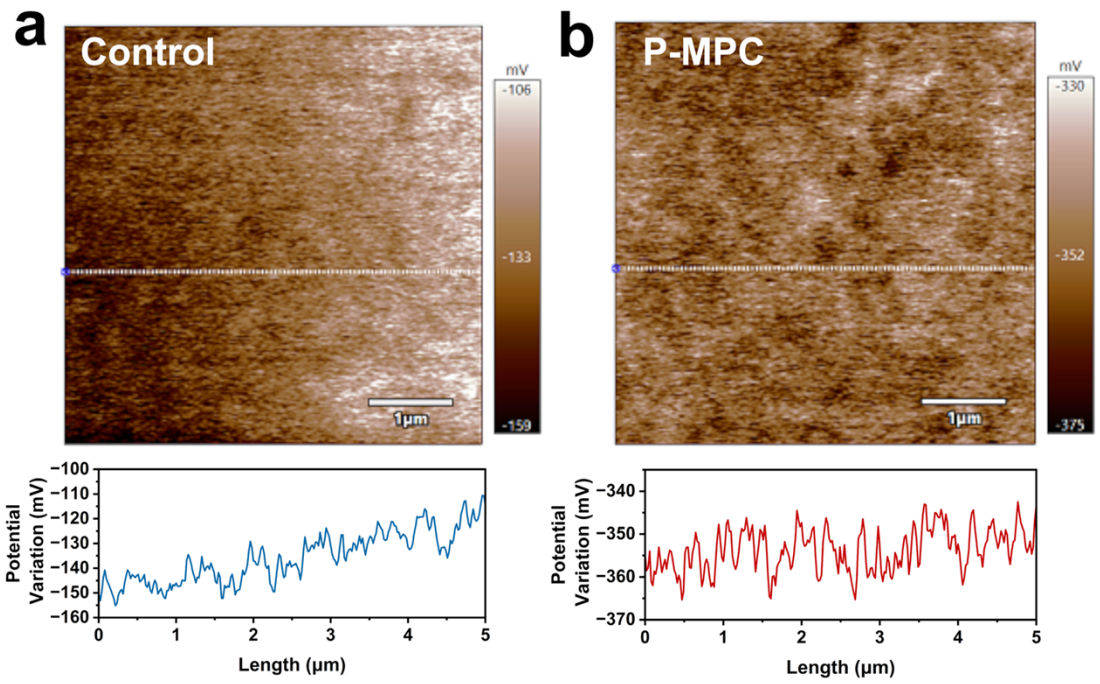

Fig. S12. (a) and (b) KPFM of contact potential differences and line profiles of the contact potential differences for control and P-MPC perovskite film, respectively.

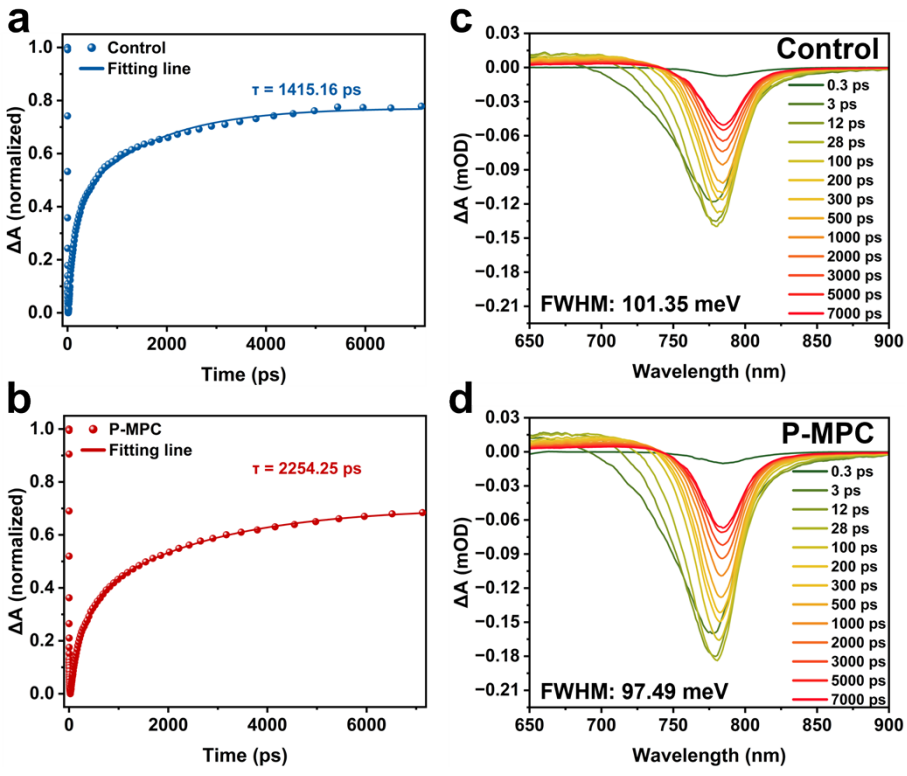

Fig. S13. (a) and (b) The bleach recovery kinetics for control and P-MPC perovskite films following the excitation at probe wavelength at 785 nm. TA spectra at different delay time of the (c) control and (d) P-MPC perovskite films.

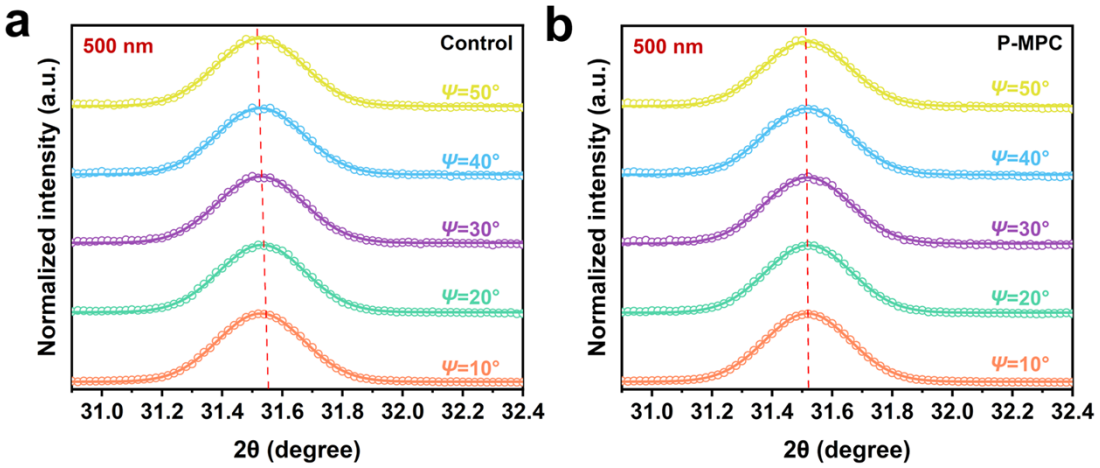

Fig. S14. GIXRD with different instrumental ϕ values (hollow circles, the measured XRD patterns; solid lines, the fitted results with Gauss function) of (a) control and (b) P-MPC perovskite films in the depth of 500 nm.

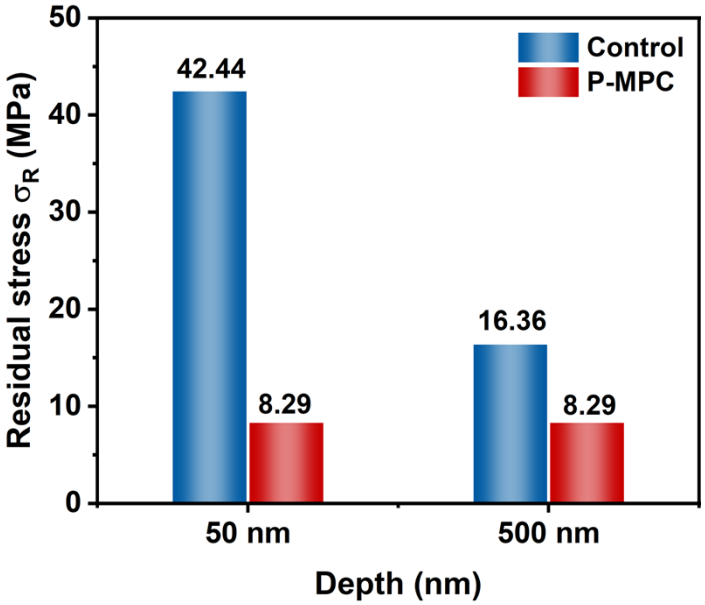

Fig. S15. Comparison of residual stress at different depths between control and P-MPC perovskite films.

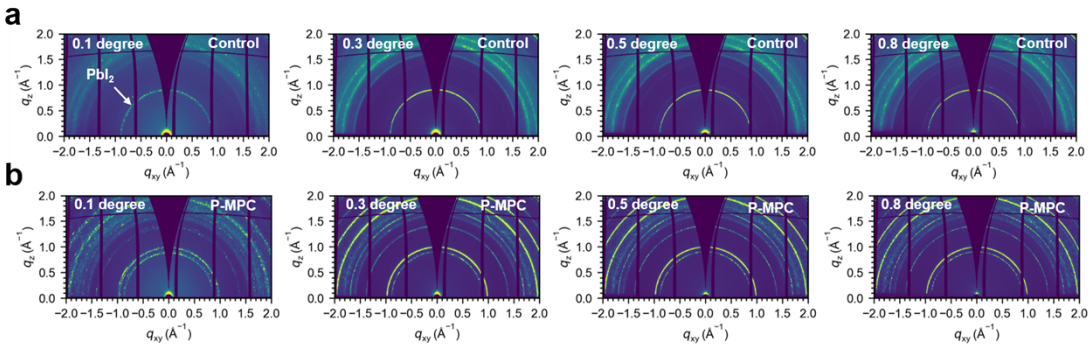

Fig. S16. 2D-GIWAXS images with different incident angle: (a) control perovskite films and (b) P-MPC perovskite films, after oven aging for 1000 h.

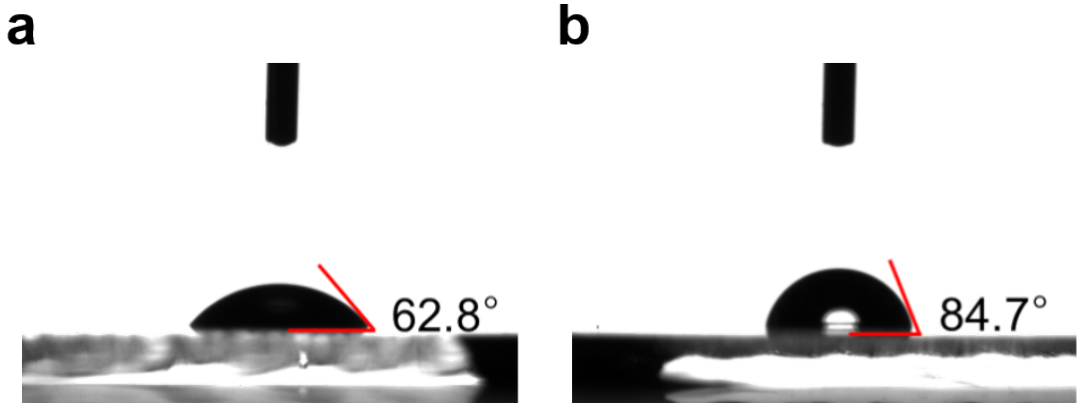

Fig. S17. Water contact angles of between control and P-MPC perovskite films.

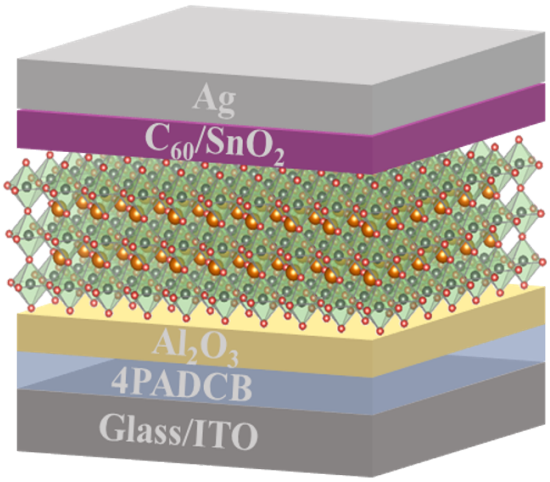

Fig. S18. Schematic illustration of p-i-n PSC based on the structure of glass/ITO/SAMs/Al_2O_3/perovskite/C_{60}/SnO_2/Ag.

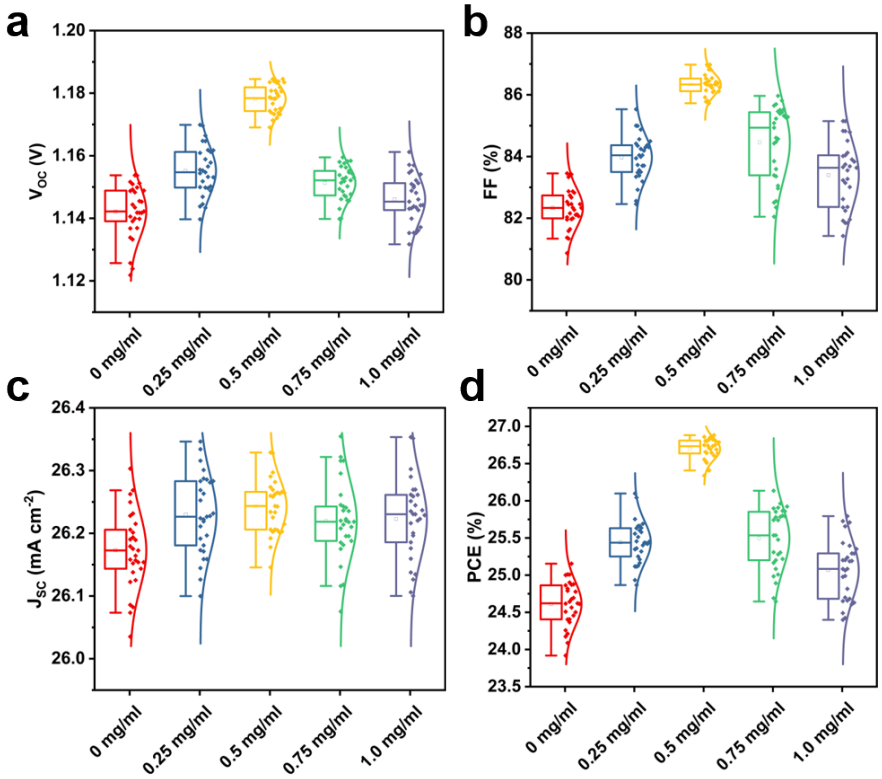

Fig. S19. (a) V_{OC} normal distribution of the devices without and with MPC. (b) FF normal distribution of the devices without and with MPC. (c) J_{SC} normal distribution of the devices without and with MPC. (d) PCE normal distribution of the devices without and with MPC.

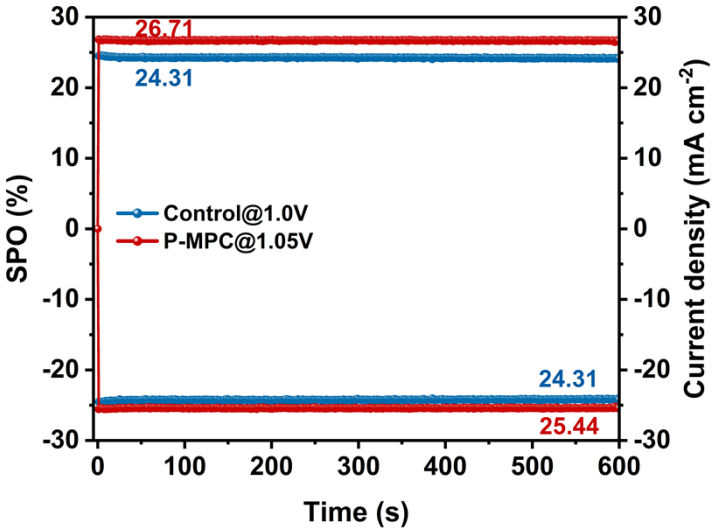

Fig. S20. Stabilized power output at the MPP for the best-performing of the control and P-MPC devices.

华南国家计量测试中心
广东省计量科学研究院
SOUTH CHINA NATIONAL CENTER OF METROLOGY
GUANGDONG INSTITUTE OF METROLOGY

校 准 证 书

CALIBRATION CERTIFICATE

证书编号 Certificate No. NYX202500560

客户名称 Name of the Customer: Shenzhen Institutes of Advanced Technology Chinese Academy of Sciences

联络信息 Contact Information: 1068 Xueyuan Avenue, Shenzhen University Town, Shenzhen

计量器具名称 Description: Perovskite Solar Cells

型号/规格 Model/Type: 2.5cm×2.5cm

制造厂 Manufacturer: Shenzhen Institutes of Advanced Technology Chinese Academy of Sciences

出厂编号 Serial No.: L-42-1

设备管理编号 Equipment No.: ----

接收日期 The date of receipt: 2025 年 09 月 10 日 (Y M D)

校准日期 The date of calibration: 2025 年 09 月 10 日 (Y M D)

发布日期 The date of issue: 2025 年 09 月 15 日 (Y M D)

批 准 Authorized by: 吴江宏

核 验 Reviewed by: 易国贤

校 准 Calibrated by: 梅书刚

证书专用章 Stamp

扫一扫查真伪

实验室地址：中国广东省东莞市石排镇东园大道石排段152号 邮政编码：523343
电话：+8620 86594172 投诉电话：+8620 36611242 E-mail：scm@scm.com.cn
Add: No.152, Shipai Section, Dongyuan Avenue, Shipai Town, Dongguan, Guangdong, China
Post Code:523343 Tel: +8620 86594172 Complaint Tel: +8620 36611242
证书真伪查询：www.scm.com.cn；cert.scm.com.cn Certificate AuthenticityIdentify: www.scm.com.cn；cert.scm.com.cn

华南国家计量测试中心
广东省计量科学研究院
SOUTH CHINA NATIONAL CENTER OF METROLOGY
GUANGDONG INSTITUTE OF METROLOGY

说　　明

证书编号 NYX202500560
Certificate No.

DIRECTIONS

1. 本中心是国家市场监督管理总局在华南地区设立的国家法定计量检定机构，本中心的质量管理体系符合ISO/IEC 17025:2017标准的要求。
This laboratory is the National Legal Metrological Verification Institution in southern China set up by the State Administration for Market Regulation. The quality system is in accordance with ISO/IEC 17025:2017.

2. 校准地点：
The location of calibration:
东莞第二检测基地A1-402

3. 本次校准使用的方法：
The method used:
JJF1622-2017 太阳电池校准规范：光电性能　C.S.for Solar Cells: Photoelectric Properties

4. 本证书中的校准结果可溯源至国际单位制（SI）单位和/或社会公用计量标准，本次校准使用以下主要计量标准器具：
The calibration results are traceable to Interational System of Units(SI) units and/or measurement standard for public service.
The major measurement standards used:

名称 Name	型号规格 Model/Type	编号 Serial No.	证书号/溯源机构 Certificate No./ Traceability to	计量特性 Metrological Characteristic
ABET 稳态太阳模拟器	SUN3000 /(300～1300)W/m²	374	NYX202400537 /本中心	光谱匹配度：A级 辐照度不均匀性：A级 辐照度不稳性：A级
标准太阳能电池	RR_257_0 / Isc：(1～200)m A	13/01/2014	GXgf2024-06295 /国家计量院	U_{rel}=2.2%， k=2
标准源表	2420 /(0～60)V,(0～3)A	4051271	DBB202503306 /本中心	电压:U_{rel}=0.1%,电流:U_{rel}=0.1%(k=2) DCV:U_{rel}=0.1%,DCA:U_{rel}=0.1%(k=2)
测量显微镜	15JE /(0~13)mm	023293	CYY202403302 /本中心	U=0.9μm (k=2)

注：1. 本证书校准结果只与受校准仪器有关。 The results relate only to the items calibrated.
Note: 2. 未经本机构书面批准，不得部分复制此证书。 This certificate shall not be reproduced except in full, without the written approval of our laboratory.
3. “客户名称”、“联络信息”由客户提供，“制造厂”、“型号规格”、“出厂编号”以及“设备编号”为仪器上标注，客户对上面内容如有异议，须在收到证书后二十个工作日内提出。
The information **Name of the Customer** and **Contact Information** are provided by customer, and the **Manufacturer**, **Model/Type**, **Serial No.** and **Equipment No.** are marked on the items.Customer shall submit any objection within 20 working days after receiving the certificate for the information above.

华南国家计量测试中心
广东省计量科学研究院
SOUTH CHINA NATIONAL CENTER OF METROLOGY
GUANGDONG INSTITUTE OF METROLOGY

校 准 结 果
RESULTS OF CALIBRATION

证书编号 NYX202500560 原始记录号 NYX202500560 第 3 页,共 4 页
Certificate No. Record No. Page of

1、外观检查： 符合要求
Apparent Inspectic Pass.

2、测试条件： 温度(25±2)℃；辐照度1000W/m^2。
Test conditions: Temperature: (25±2)℃; Irradiance: 1000W/m^2.

3、电流-电压特性曲线和功率-电压特性曲线：
I-V and P-V curves:

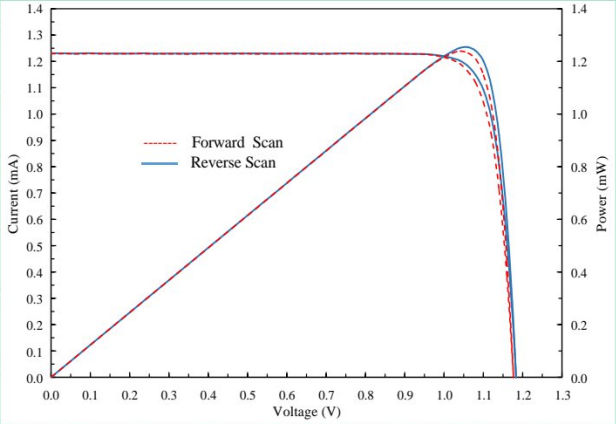

图1 电流-电压特性曲线和功率-电压特性曲线
Figure1 I-V and P-V characteristic curves

4、光电性能参数(反扫以及正扫)：
Results of photoelectric properties(Reverse scan and forward scan):

表1(Table 1)

正反扫	面积	短路电流密度J_{sc}	短路电流I_{sc}	开路电压V_{oc}	填充因子FF	最大功率P_m	最佳工作电流I_m	最佳工作电压V_m	转换效率η
Reverse/ Forward	Area	Short ciruit current density	Short ciruit current	Open circuit voltage	Fill factor	Maximum power	Optimum working current	Optimum working voltage	Efficiency
	cm^2	mA/cm^2	mA	V	%	mW	mA	V	%
Reverse	0.0470	26.16	1.230	1.183	86.23	1.254	1.183	1.060	26.69
Forward	0.0470	26.15	1.229	1.176	85.72	1.239	1.191	1.040	26.36

Fig. S21. Independent efficiency certification of perovskite solar cells by an accredited institute of South China National Center of Metrology.

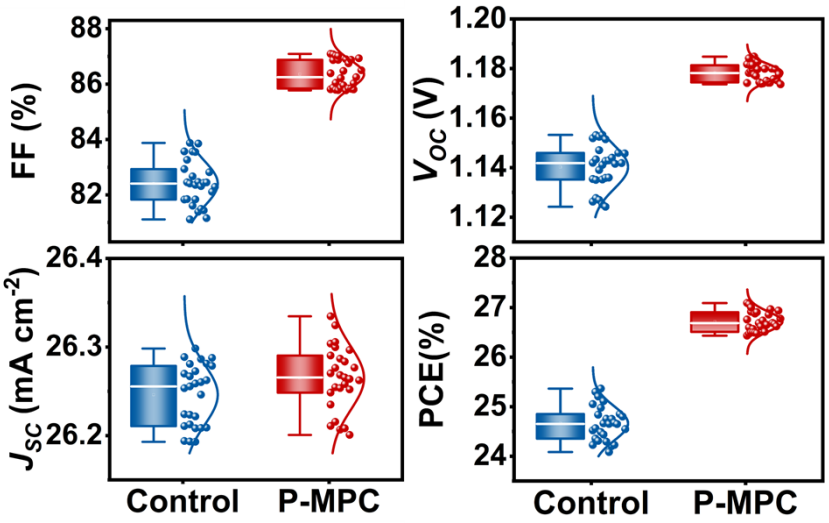

Fig. S22. Statistical photovoltaic parameters of 30 PSCs based on the control and P-MPC devices.

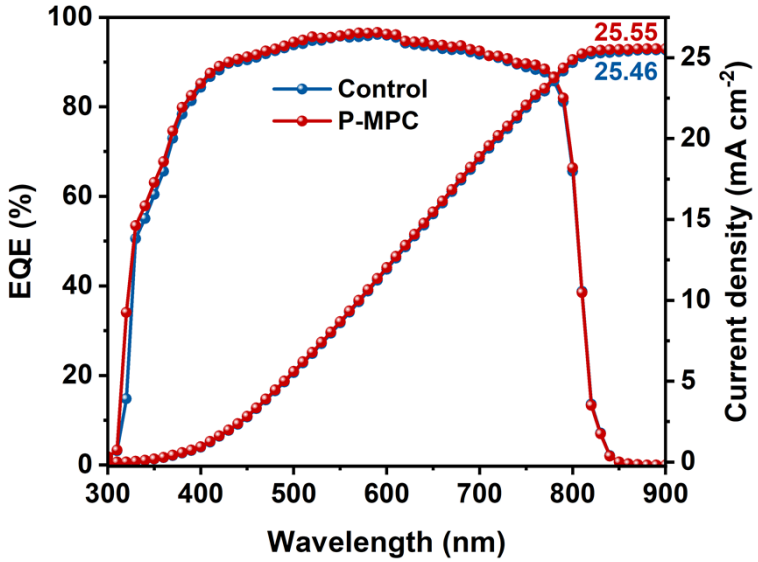

Fig. S23. EQE spectra and integrated current (J_{sc}) of the control and P-MPC champion device.

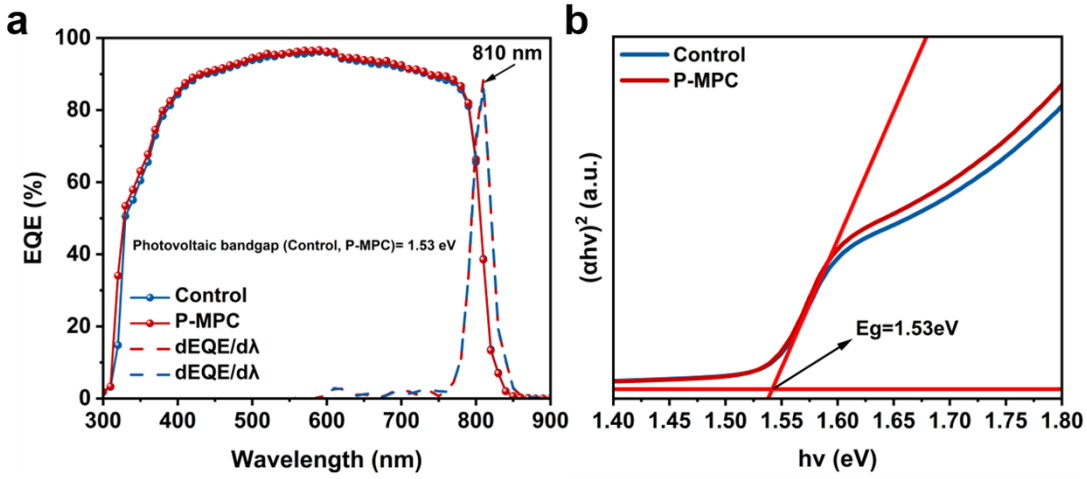

Fig. S24. (a) Eg estimation obtained from the inflection point of the EQE spectra by locating the maximum point (λg) of the Gaussian-like derivate $\partial EQE/\partial\lambda$. (b) Tauc plots of UV-vis absorption spectra of control and MCP perovskite films.

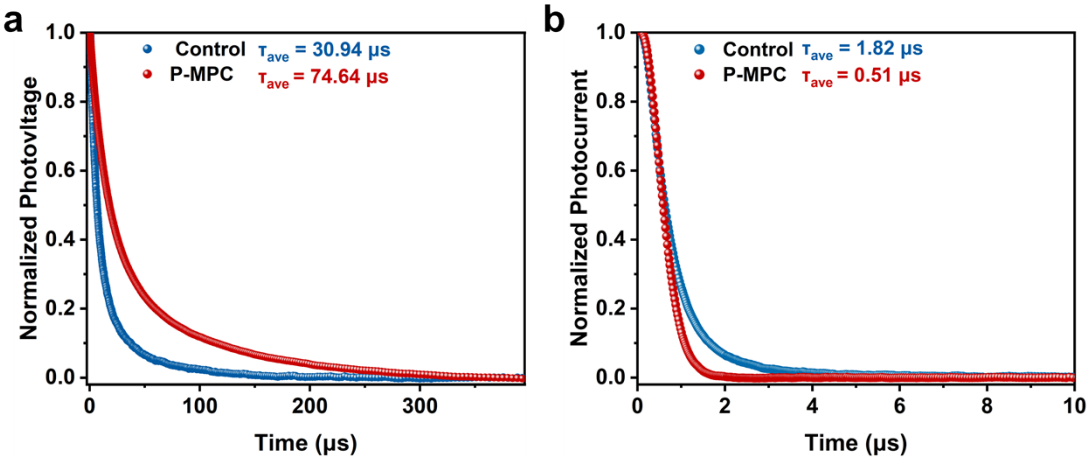

Fig. S25. (a) TPV and (b) TPC spectra for control and P-MPC devices.

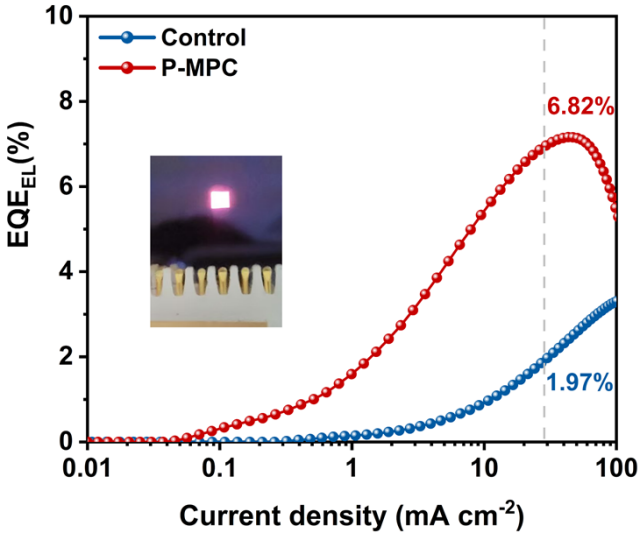

Fig. S26. External quantum efficiency of electroluminescence (EQE_{EL}) measurements of control and P-MPC PSCs.

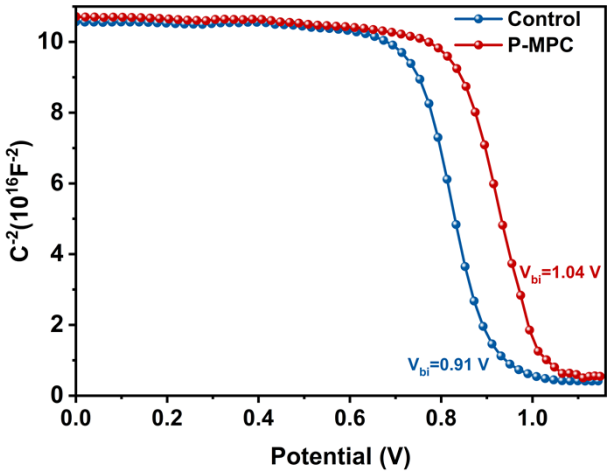

Fig. S27. Mott-Schottky plots for control and P-MPC devices.

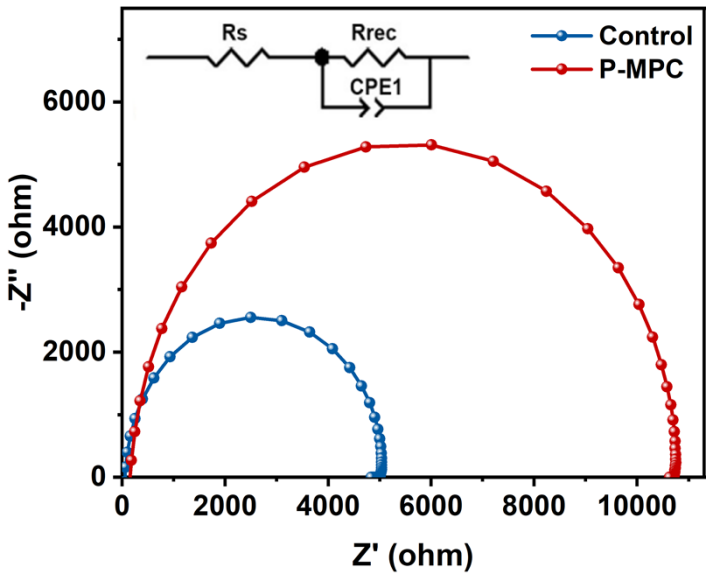

Fig. S28. Electrochemical impedance spectroscopy of the corresponding devices. Inset shows its equivalent circuit.

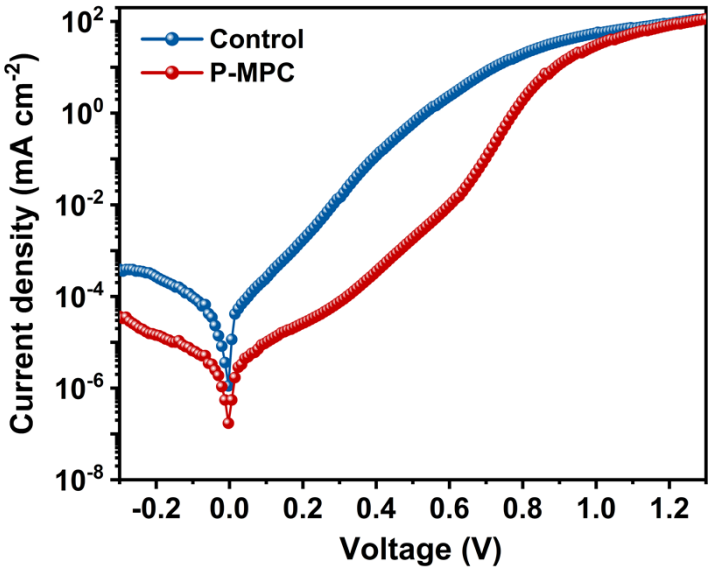

Fig. S29. Dark *J*–*V* curves of the control and P-MPC devises.

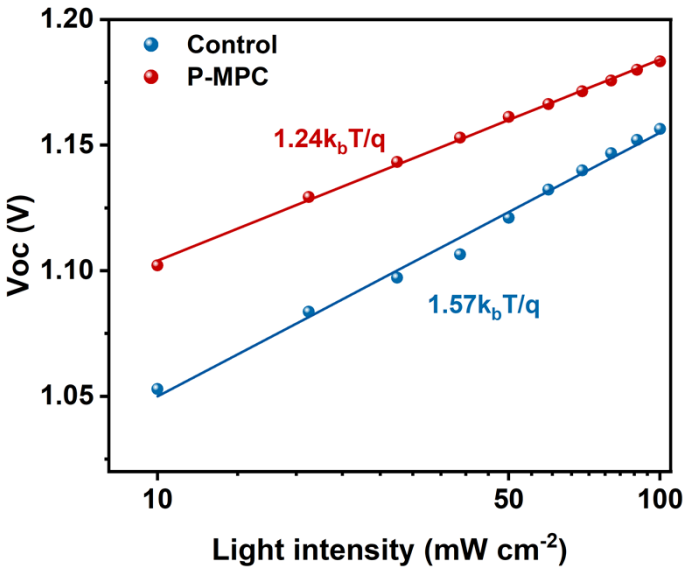

Fig. S30. Light intensity dependence of V_{OC} of the control and P-MPC devices.

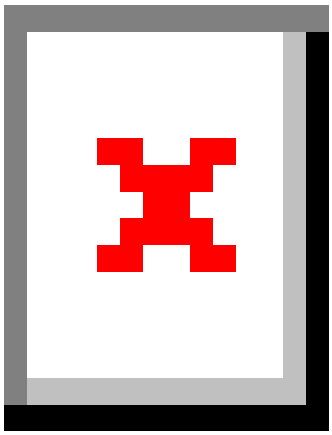

Fig. S31. Schematic illustration of laser scribing by P1, P2, and P3 lines for PSC modules.

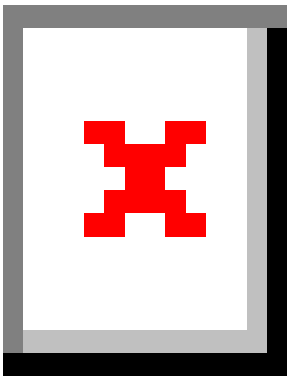

Fig. S32. (a) Schematic illustration and (b) SEM top-view image of the perovskite solar module showing the P1-P2-P3 parameters.

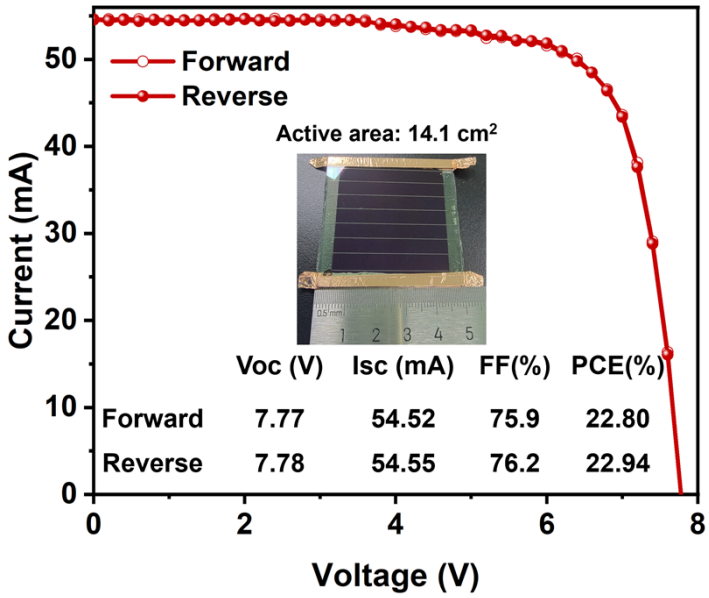

Fig. S33. *J–V* curve of the champion perovskite solar module with an active area of 14.1 cm^2.

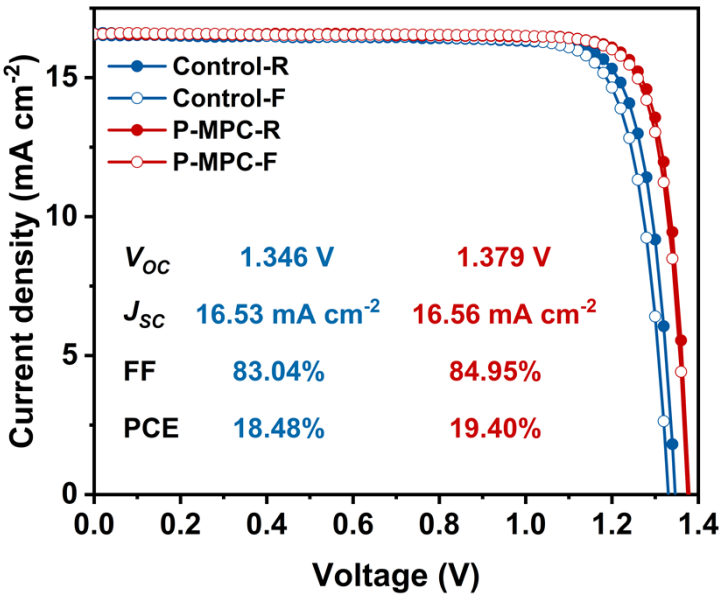

Fig. S34. *J-V* curves of 1.85 eV PSCs without or with P-MPC

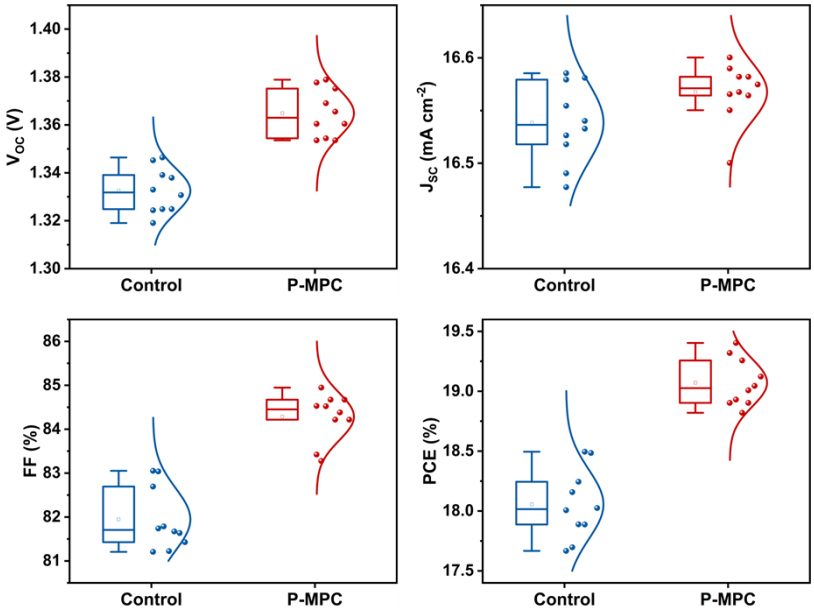

Fig. S35. Device photovoltaic parameter statistics. V_{OC}, J_{SC}, FF and PCE distribution of 10 independent devices (1.85 eV).

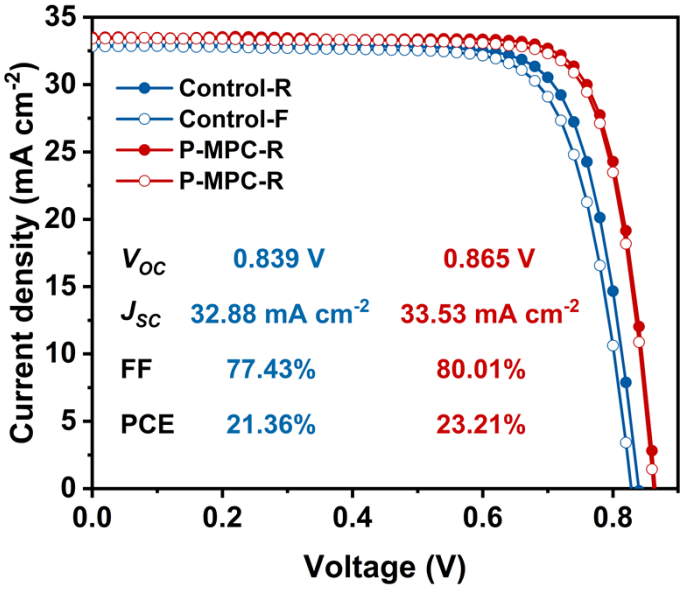

Fig. S36. *J-V* curves of 1.25 eV PSCs without or with P-MPC.

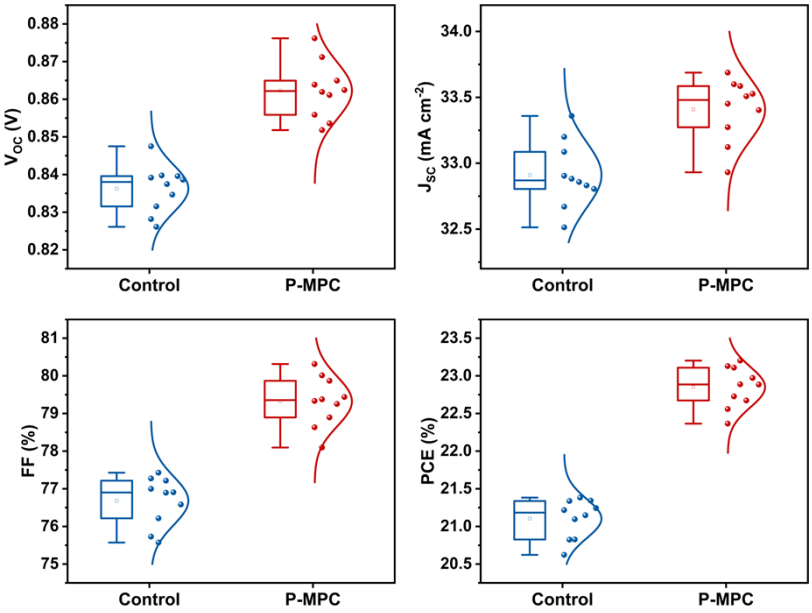

Fig. S37. Device photovoltaic parameter statistics. V_{OC}, J_{SC}, FF and PCE distribution of 10 independent devices (1.25 eV).

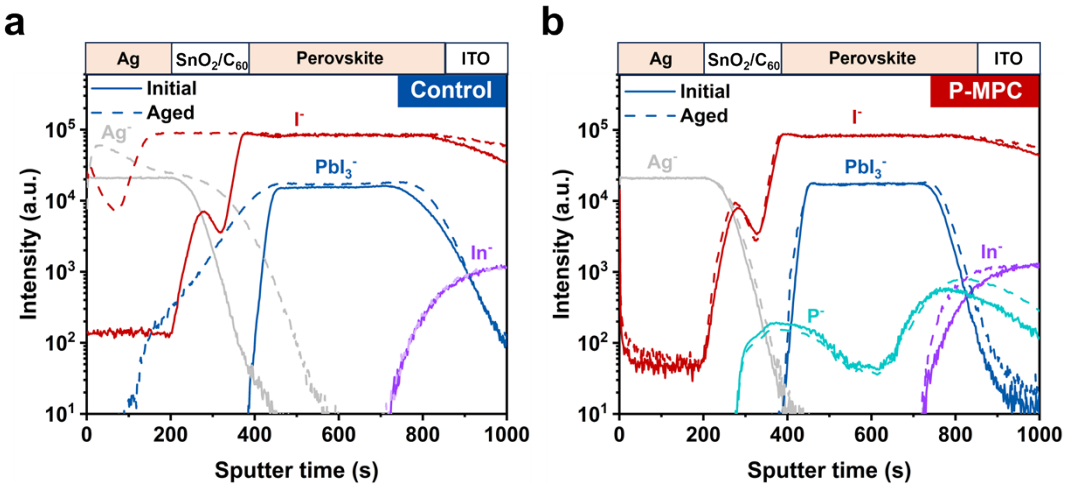

Fig. S38. ToF-SIMS analysis of (a) control and (b) P-MPC devices before and after aging under continuous illumination at for 500 h.

Table S1. Time-resolved PL data of perovskite films.

Device	A_1	τ_1（ns）	A_2	τ_2（ns）	τ_{avg}
Control	7168.708	8.934	2574.258	154.911	134.69
P-MPC	5607.157	12.638	3925.691	334.051	317.62

Table S2. Fitting parameters for TAS of bi-exponential decay fits of Control and P-MPC perovskite films.

Device	A_1	τ_1（ns）	A_2	τ_2（ns）	τ_{avg}
Control	-0.45	120.85	-0.32	1532.91	1415.16
P-MPC	-0.32	292.32	-0.39	2446.59	2254.25

Table S3. Instrumental angles (Ψ, ω, Φ) set for (012) crystal plane in different depths of GIXRD residual stress measurements.

Depth (nm)	（hkl）	Ψ (°)	*ω* (°)	Φ (°)
50	（012）	10	0.3151	-17.4592
		20	0.3303	-32.0793
		30	0.3588	-51.0211
		40	0.4063	-66.8129
		50	0.4855	-70.3292
500	（012）	10	3.5270	-38.5979
		20	3.7233	-57.9712
		30	4.0967	-67.4958
		40	4.7471	-73.0964
		50	5.9242	-77.1963

Table S4. The slope of the residual strain fitting line and strain values for the perovskite films with and without P-MPC at the depth of 50 nm and 500 nm.

Depth (nm)	Films	Slope	Strain (MPa)
50 nm	Control	-0.179	42.44
	P-MPC	-0.035	8.29
500 nm	Control	-0.069	16.36
	P-MPC	-0.035	8.29

Table S5. Photovoltaic parameters for PSCs with different concentrations of MPC.

MPC	V_{OC} (V)	J_{SC} (mA cm^{-2})	FF (%)	PCE (%)
0 mg/ml	1.142	26.17	82.33	24.61
0.25 mg/ml	1.155	26.23	83.97	25.44
0.5 mg/ml	1.178	26.24	86.24	26.65
0.75 mg/ml	1.151	26.21	84.45	25.48
1 mg/ml	1.146	26.23	83.40	25.07

Table S6. Photovoltaic parameters of control and P-MPC PSCs.

Device type	Scan direction	V_{OC} (V)	J_{SC} (mA/cm^2)	FF (%)	PCE (%)
Control	FS	1.145	26.24	81.59	24.51
	RS	1.153	26.22	83.88	25.36
P-MPC	FS	1.180	26.26	86.24	26.72
	RS	1.184	26.27	87.09	27.09

Table S7. Summary of the photovoltaic performance of PSC in this work and other literature related to the crystallization regulation and chemical passivation of perovskite. PCE[a] represents the certified PCE of third-party organizations. Please note that passivation layers in the following devices have been omitted.

Device structure	Additive	V_{OC} (V)	J_{SC} (mAcm^{-2})	FF (%)	PCE (%)	Ref.
ITO/MeO-2PACz/$Cs_{0.05}(FA_{0.98}MA_{0.02})_{0.95}Pb(I_{0.98}Br_{0.02})_3$ /$PC_{61}BM$/BCP/Ag	b-poly(1,1-difluoroethylene	1.174	24.84	83.21	24.24[a]	Science, 2023, 379, 399.
ITO/DC-PA/$Cs_{0.06}MA_{0.14}FA_{0.80}PbI_3$/$C_{60}$/BCP/Ag	4-guanidinobenzoic acid hydrochloride	1.190	24.47	84.2	24.5[a]	Nat. Photonics, 2023, 17, 478.
ITO/NiO_x/PTAA/Al2O3/$Cs_{0.05}FA_{0.95}PbI_3$/PCBM/BCP/Ag	2-aminoindan hydrochloride	1.173	25.68	81.63	24.6[a]	Nat. Energy, 2023, 8, 946.
ITO/SnO2/FA0.95Cs0.05PbI3/Spiro-OMeTAD/Au	Pentanamidinehydrochlori de	1.15	26.55	81.95	25.02[a]	Nature, 2023, 620, 323.
ITO/perovskite/$PC_{61}BM$/BCP/Ag	(4-(2,7-dibromo-9,9-dimethylacridin 10(9H)-yl)butyl)phosphonic acid	1.189	25.66	83.24	25.39[a]	Nature, 2023, 620, 545.
FTO/SnO_2/$FAPbI_3$/spiro-OMeTAD/Au	hexafluorobenzene	1.193	26.66	81.31	25.8[a]	Nature, 2023, 623, 531.
ITO/PTAA/$FA_{0.95}Cs_{0.05}PbI_3$/C_{60}/BCP/Ag	1-(phenylsulfonyl)pyrrole	1.153	26.50	84.46	25.81[a]	Nature, 2023, 624, 557.
FTO/Me-4PACz/$Cs_{0.05}MA_{0.1}FA_{0.85}PbI_3$/$C_{60}$/$SnO_x$/Ag	4-chlorobenzenesulfonate	1.174	26.13	85.2	26.15[a]	Science, 2024, 384, 189.
ITO/SnO_2/$FA_{0.94}Cs_{0.06}PbI_3$/Spiro-OMeTAD/Au	acetate anions	1.186	26.43	84.98	26.64[a]	Nature, 2024, 635, 82.
ITO/PTAA/$Cs_{0.05}FA_{0.85}MA_{0.1}Pb(I_{0.97}Br_{0.03})_3$/$C_{60}$/ BCP/Cu	tris(2,4,6-trimethyl-3-(pyridin-3 yl)phenyl)borane	1.191	25.15	85.38	25.58[a]	Nat. Photonics, 2025, 19, 28.
ITO/Me-2PACz/$Cs_{0.05}MA_{0.1}FA_{0.85}PbI_3$/$C_{60}$/BCP/Cu	eutectic molecule	1.174	25.80	84.86	25.7[a]	Nat. Photonics, 2025, 19, 258.
ITO/4PADCB/Al_2O_3/$FA_{0.95}Cs_{0.05}PbI_3$/C_{60}/SnO_2/Ag	**P-MPC**	**1.183**	**26.16**	**86.23**	**26.69[a]**	**This work**

Supplementary References

1. J. Zhang and T. Lu, *Phys. Chem. Chem. Phys.*, 2021, **23**, 20323-20328.
2. W. Humphrey, A. Dalke and K. Schulten, *J. Mol. Graphics.*, 1996, **14**, 33-38.
3. J. P. Perdew, K. Burke and M. Ernzerhof, *Phys. Rev. Lett.*, 1996, **77**, 3865-3868.
4. B. Hammer, L. B. Hansen and J. K. Nørskov, *Phys. Rev. B*, 1999, **59**, 7413-7421.
5. S. Grimme, *J. Comput. Chem.*, 2006, **27**, 1787-1799.
6. P. E. Blöchl, *Phys. Rev. B*, 1994, **50**, 17953-17979.
7. H. Wang, C. Zhu, L. Liu, S. Ma, P. Liu, J. Wu, C. Shi, Q. Du, Y. Hao, S. Xiang, H. Chen, P. Chen, Y. Bai, H. Zhou, Y. Li and Q. Chen, *Adv. Mater.*, 2019, **31**, 1904408.
8. M. Ghasemi Hajiabadi, M. Zamanian and D. Souri, *Ceram. Int.*, 2019, **45**, 14084-14089.
9. R. A. McKee, *Sol. State Ion.*, 1981, **5**, 133-136.